Earth, Planets and Space

FULL PAPER

Open Access

Monitoring hydraulic stimulation using telluric sounding

Nigel Rees[1*] , Graham Heinson[2] and Dennis Conway[2]

Abstract

The telluric sounding (TS) method is introduced as a potential tool for monitoring hydraulic fracturing at depth. The advantage of this technique is that it requires only the measurement of electric fields, which are cheap and easy when compared with magnetotelluric measurements. Additionally, the transfer function between electric fields from two locations is essentially the identity matrix for a 1D Earth no matter what the vertical structure. Therefore, changes in the earth resulting from the introduction of conductive bodies underneath one of these sites can be associated with deviations away from the identity matrix, with static shift appearing as a galvanic multiplier at all periods. Singular value decomposition and eigenvalue analysis can reduce the complexity of the resulting telluric distortion matrix to simpler parameters that can be visualised in the form of Mohr circles. This technique would be useful in constraining the lateral extent of resistivity changes. We test the viability of utilising the TS method for monitoring on both a synthetic dataset and for a hydraulic stimulation of an enhanced geothermal system case study conducted in Paralana, South Australia. The synthetic data example shows small but consistent changes in the transfer functions associated with hydraulic stimulation, with grids of Mohr circles introduced as a useful diagnostic tool for visualising the extent of fluid movement. The Paralana electric field data were relatively noisy and affected by the dead band making the analysis of transfer functions difficult. However, changes in the order of 5% were observed from 5 s to longer periods. We conclude that deep monitoring using the TS method is marginal at depths in the order of 4 km and that in order to have meaningful interpretations, electric field data need to be of a high quality with low levels of site noise.

Keywords: Telluric sounding, Hydraulic stimulation, Monitoring, Transfer functions

Introduction

The telluric sounding (TS) method was introduced in the 1960s and involves simultaneously recording the horizontal components of electric fields (**E**) at different sites (Berdičevskij and Keller 1965; Yungul 1966). The measured **E** can be affected by galvanic distortion, which is caused by gradients in electrical conductivity associated with near-surface heterogeneities (Chave and Smith 1994). The accumulation of charge at conductivity boundaries strongly alters **E** (Groom and Bailey 1989). This local distortion of **E** can be described by a real-valued second-rank tensor **D** that relates the electric field measured at a local (**E**$_M$) and regional (**E**$_B$) site according to (Chave and Jones 2012)

$$\mathbf{E}_M = \mathbf{D}\mathbf{E}_B \tag{1}$$

where

$$\mathbf{D} = \begin{bmatrix} D_{xx} & D_{xy} \\ D_{yx} & D_{yy} \end{bmatrix}. \tag{2}$$

In this case, **D** is relative to axes X and Y, typically north and east. Introducing a rotation matrix $\mathbf{R}(\theta)$,

$$\mathbf{R}(\theta) = \begin{bmatrix} \cos\theta & \sin\theta \\ -\sin\theta & \cos\theta \end{bmatrix}, \tag{3}$$

and the transpose $\mathbf{R}^{\mathbf{T}}(\theta)$, the value of **D** relative to axes X' and Y' (which are rotated θ' clockwise from north and east) is given by the matrix $\mathbf{D}'$ (Lilley 2015)

$$\begin{bmatrix} D'_{xx} & D'_{xy} \\ D'_{yx} & D'_{yy} \end{bmatrix} = \mathbf{R}(-\theta') \begin{bmatrix} D_{xx} & D_{xy} \\ D_{yx} & D_{yy} \end{bmatrix} \mathbf{R}(\theta'). \tag{4}$$

*Correspondence: nigel.rees@anu.edu.au
[1] The Australian National University, Canberra, ACT 0200, Australia
Full list of author information is available at the end of the article

Rees *et al. Earth, Planets and Space* (2018) 70:7

Page 2 of 12

For a 1D Earth, the distortion matrix will be the identity matrix. The presence of galvanic distortion will be manifest as an amplitude shift, and a twist and shear operation (Lilley 2015). For 2D structures, the distortion matrix can be rotated to reflect the changes in **E** along and across strike.

Targets for hydraulic stimulation are generally in sedimentary basins that are laterally extensive, and for most of the bandwidth the responses are 1D. The injection of conductive fluids into the subsurface will alter the telluric distortion matrix which can be mapped to show the lateral constraints of fluid migration. Lilley (2015) proposed the application of both eigenvalue analysis (EA) and singular value decomposition (SVD) on the telluric distortion matrix, with Mohr diagrams introduced as a versatile way of visualising properties of the matrix. These diagrams can be used to determine the extent to which the matrix is diagnostic of 1D, 2D or 3D geological structure as well as determining a strike direction (with 90° ambiguity) and a relative amplitude change. Grids of Mohr circles can show where the greater amplitude changes occur at depth and may be used to determine the extent to which fluid has migrated from the injection point.

Following from Lilley (2015), EA of the telluric distortion matrix involves finding a direction of $\mathbf{E}_M$ for which the change in $\mathbf{E}_B$ is in the same direction, with the eigenvalue of the direction giving the gain of the process. When real eigenvectors exist, the characteristic equation for **D**,

$$\zeta^2 - (D_{xx} + D_{yy})\zeta + D_{xx}D_{yy} - D_{xy}D_{yx} = 0, \qquad (5)$$

can be solved for the two eigenvalues ζ_1 and ζ_2 with solutions

$$\zeta_1, \zeta_2 = \frac{1}{2}(D_{xx} + D_{yy})$$
$$\pm \frac{1}{2}\sqrt{(D_{xx} + D_{yy})^2 + 4(D_{xy}D_{yx} - D_{xx}D_{yy})}. \qquad (6)$$

Eigenvectors can then be found corresponding to these eigenvalues. The solutions to EA can be plotted on a Mohr circle with centre $[(D_{xx} + D_{yy})/2, (D_{xy} - D_{yx})/2]$ and radius $r = \sqrt{(D_{xy} + D_{yx})^2 + (D_{xx} - D_{yy})^2}$. Axes for D'_{yx} and D'_{yy} can also be plotted to display the variation with axis rotation of all components of $\mathbf{D}'$. Figure 1a shows an example of such a Mohr diagram, where P represents the observed point, H and J mark the EA positions and C represents the centre of the circle. The eigenvalues are the D'_{xx} axis values of H and J.

The SVD of **D** produces a rotation for the axes at the regional site B and a different rotation for the axes at local site M. Therefore, a change in **E** at rotated site B produces a change in **E** along the corresponding but differently rotated axis at site M, with the change generally amplified or attenuated (Lilley 2015). This rotation of the local and regional axes reduces the telluric distortion tensor to an ideal 2D form. The results of SVD can also be displayed on a Mohr diagram as shown in Fig. 1b. Here, OG and OF represent the greater and lesser singular values, P is the observed point and C is the centre. Grids of SVD Mohr circles can show the magnitudes and directions of the injected near surface anomaly. For a detailed explanation on the theory of EA, SVD and Mohr diagrams related to the telluric distortion matrix, the reader is referred to Lilley (1993, 2012, 2015).
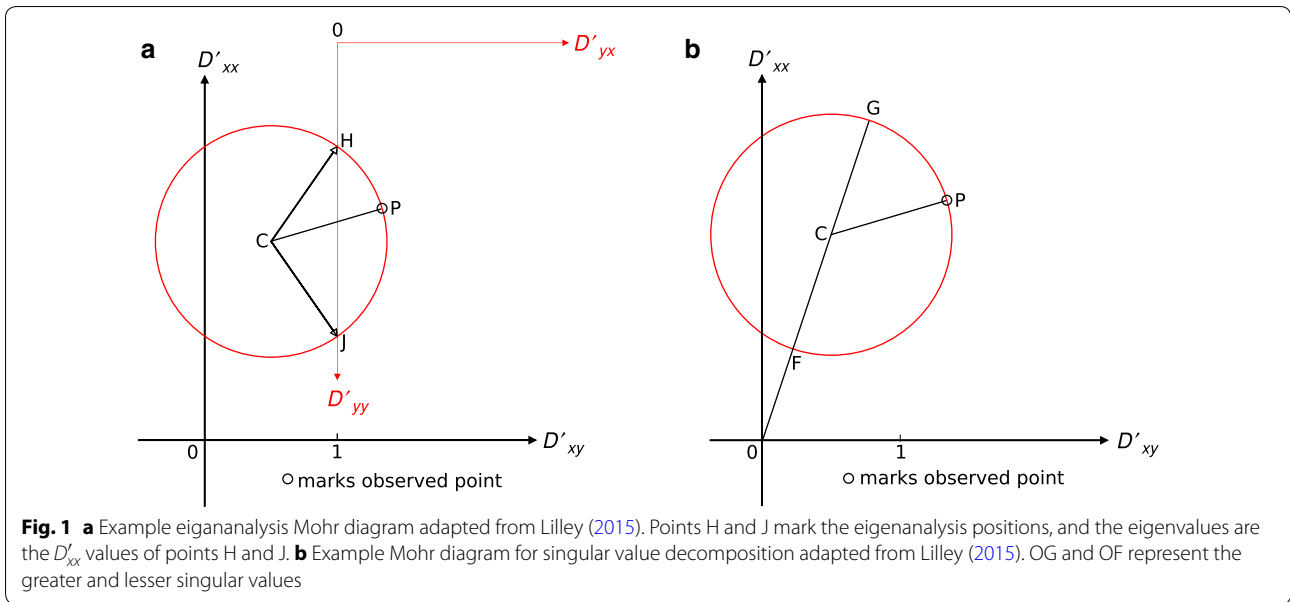
The goal of this study is to test the viability of utilising the TS method for monitoring hydraulic stimulation at depth. Ideally we would like to be able to constrain the spatial and temporal dimensions of resistivity changes. Spatial changes can be constrained laterally from using multiple sites, and depths can be estimated given resistivity data to map periods to depths. One advantage of the TS method is that it is relatively easy to measure **E** with many dipoles and multi-channel systems and therefore **E** arrays could be deployed for continuous monitoring. Additionally, hydraulic stimulation targets are generally laterally extensive sedimentary basins where **E** transfer functions are essentially the identity matrix. Therefore, monitoring would involve plotting deviations relative to the identity matrix, with static shift appearing as a galvanic multiplier at all periods. The impedance on the other hand has real and imaginary components that vary with frequency. Finally, the TS method is relatively low cost when compared with traditional magnetotelluric measurements and may prove a simple and favourable method for monitoring fluid movement.

3D feasibility study

A 3D feasibility study was conducted to test the viability of the TS method for monitoring conductive change at depth. The 3D forward modelling code of Mackie et al. (1993) was used to create a baseline resistivity structure as shown in Fig. 2. The baseline resistivity model consisted of a 10 Ωm conductive layer down to 0.8 km, a 50 Ω m layer from 0.8 to 2 km, a 100 Ωm layer from 2 to 4.5 km and finally a 1000 Ωm layer from 4.5 to 1200 km. The stimulation model introduces a 1 Ωm conductive block at 3.6 km depth, with volumetric dimensions of $3 \times 1 \times 0.4$ km.

3D forward modelling for both base and stimulation resistivity structures produced classical MT responses (see Additional file 1). From the forward modelling code and the following equation, we calculate **D**

$$\mathbf{Z}_M = \mathbf{D}\mathbf{Z}_B \qquad (7)$$

Rees *et al. Earth, Planets and Space* (2018) 70:7

Page 3 of 12

Fig. 1 a Example eigananalysis Mohr diagram adapted from Lilley (2015). Points H and J mark the eigenanalysis positions, and the eigenvalues are the D'_{xx} values of points H and J. **b** Example Mohr diagram for singular value decomposition adapted from Lilley (2015). OG and OF represent the greater and lesser singular values

where $\mathbf{Z}_M$ and $\mathbf{Z}_B$ are the local and regional site impedance tensors, respectively, and **D** is a 2×2 matrix. If we multiply both sides by a regional and uniform **B** field (i.e. $\mathbf{B}_B = \mathbf{B}_M$), then

$$\mathbf{Z}_M\mathbf{B} = \mathbf{D}\mathbf{Z}_B\mathbf{B}. \tag{8}$$

As $\mathbf{E} = \mathbf{ZB}$, Eq. 8 can be written as

$$\mathbf{E}_M = \mathbf{D}\mathbf{E}_B. \tag{9}$$

Therefore, the distortion matrix calculated from the impedance tensors is the same as the impedance matrix calculated from the electric fields.

Figures 3, 4, 5 and 6 show each component of the resultant transfer functions (D_{xx}, D_{xy}, D_{yx}, D_{yy}; here the first subscript represents the local site and the second the reference site) between the $\mathbf{E}_B$ and $\mathbf{E}_M$ sites for the six lines in the synthetic grid.

The baseline transfer functions represent the identity matrix, where D_{xx} and D_{yy} are 1 and D_{xy} and D_{yx} are 0 for all periods. The stimulation D_{xx} and D_{yy} show changes of between 1 and 2%, with these changes occurring from about 5 s and continuing to longer periods. The changes in D_{yy} are slightly larger when compared with D_{xx}, and the stations furthest away from the injection (e.g. station 59) show negligible changes. The changes in D_{xy} and D_{yx} are generally less than 1%.

Changes in transfer functions (and hence telluric distortion matrices) can be analysed using SVD and EA and plotted onto Mohr circles grids [see Lilley (2015)]. Such a grid is shown in Fig. 7, where SVD analysis was performed on telluric distortion matrices comparing $\mathbf{E}_B$ and $\mathbf{E}_M$ along Line 3 during stimulation. The grey

vertical and horizontal lines represent the D'_{xx} and D'_{xy} axes, respectively. The black radius interacts with the red circle at the observed point. The Mohr circles increase in diameter for stations surrounding the 1 Ω m conductive body (stations 32–34) at periods of 3 s and greater. The size of the Mohr circles progressively become smaller and approach the identity matrix moving further east from station 34. Similar grids can be plotted using EA as shown in Fig. 8. Here the dashed red lines are the D'_{yy} axis and the two black radii represent the eigenvalues. Notice that for the sites surrounding the conductive zone, the eigenvalues are real and different and the eigenvectors are orthogonal which is a representation of the 2D case [see Fig. 4 from Lilley (2015) for a detailed explanation on Mohr diagram eigenanalysis using different matrices as examples].

Another interesting way of viewing telluric distortion matrix changes is by mapping Mohr circles at specific periods for each site in the array. Such a representation is shown in Fig. 9, where SVD Mohr circles are drawn for every site at a period of 5 s. The 1 Ωm conductive body lies between Lines 3 and 4, and the Mohr circles surrounding the body increase in size and amplitude. Line 6 is the furthest away from the conductive body, and all Mohr circles on this line are the identity matrix. The edge of the conductive body is horizontally well marked along lines 2 and 3. However, the boundary is not as well marked when you look vertically in Fig. 9, where the effects of the conductive block are also seen on Lines 1 and 4. This is also noticeable in Fig. 6 where the transfer functions show poorer cross-line constraints on the lateral extent. Figure 3 shows slightly better cross-line

Rees *et al. Earth, Planets and Space* (2018) 70:7

Page 4 of 12
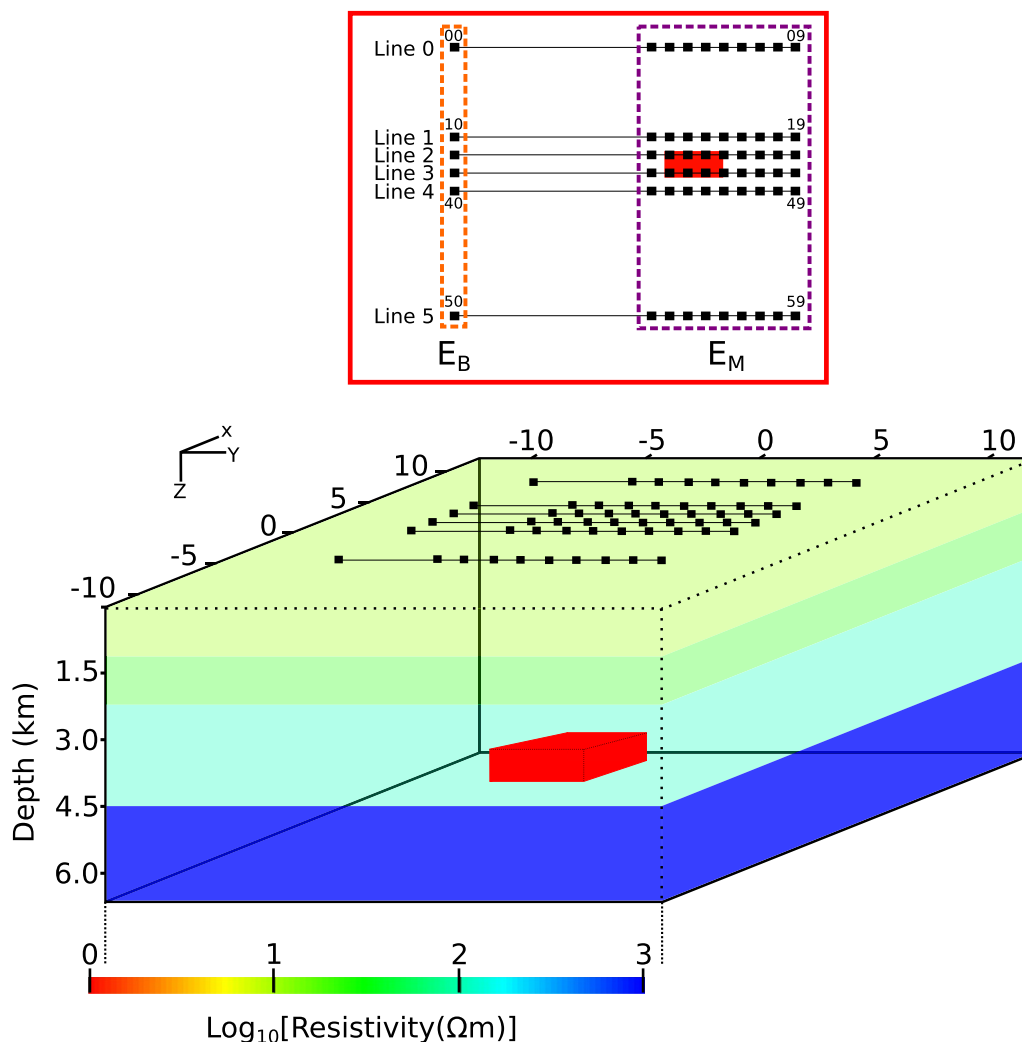
Fig. 2 Resistivity model used for the 3D synthetic forward modelling study. The red box shows a birds eye view of the six lines, with each black square representing one site. The orange dashed box shows the respective base sites ($\mathbf{E}_B$) used for each line, and the dashed purple box shows the measured sites ($\mathbf{E}_M$). The location of the red conductive block at 3.6 km depth is shown
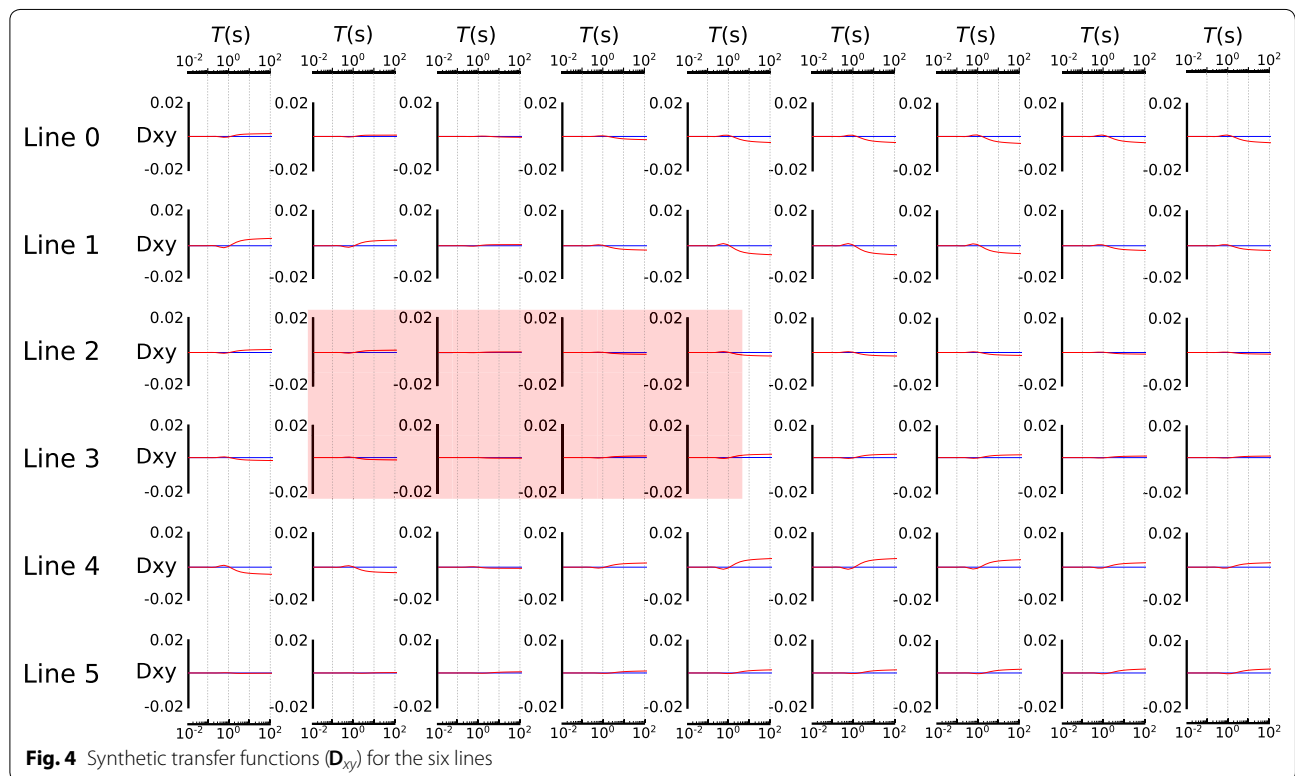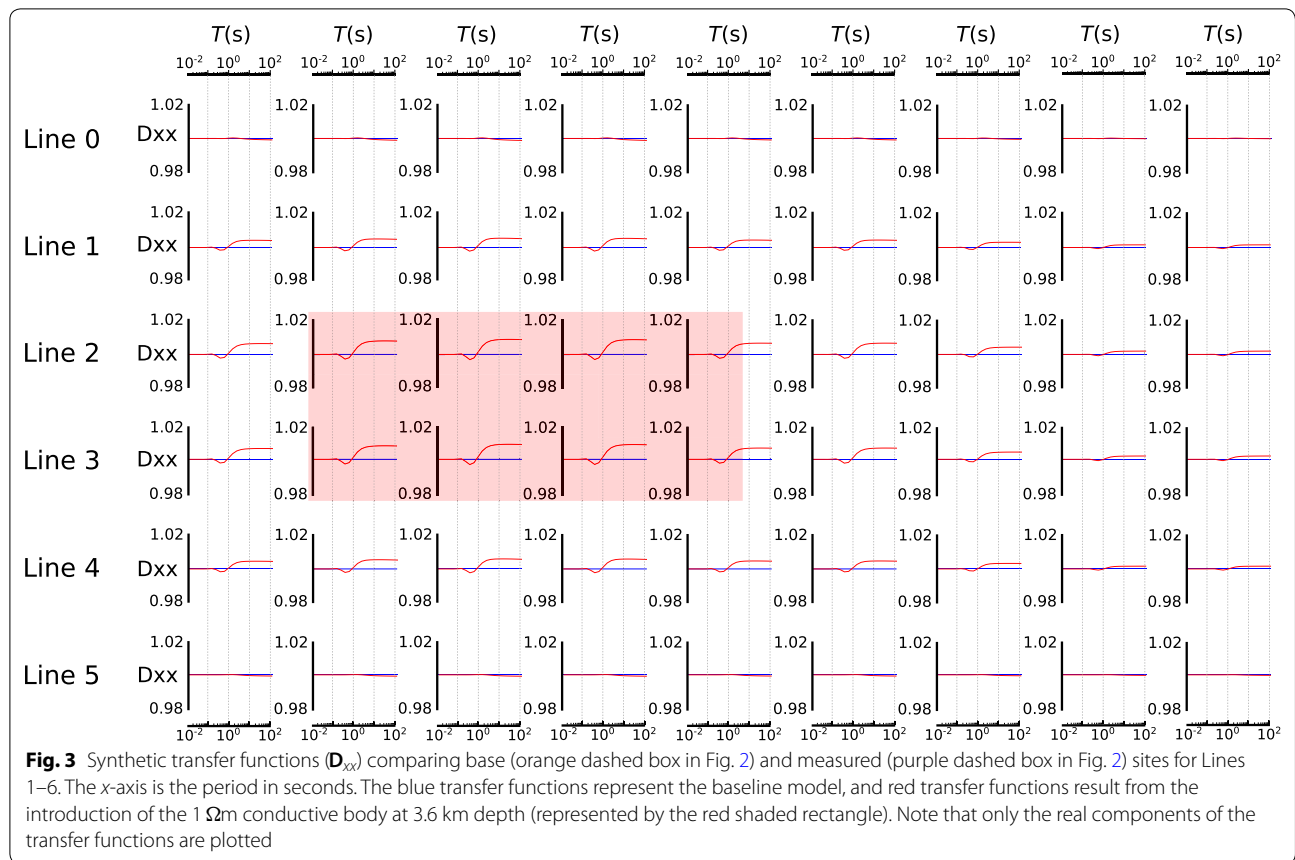
constraints, where Lines 1 and 4 show reduced maximums in transfer functions when compared with Lines 2 and 3.
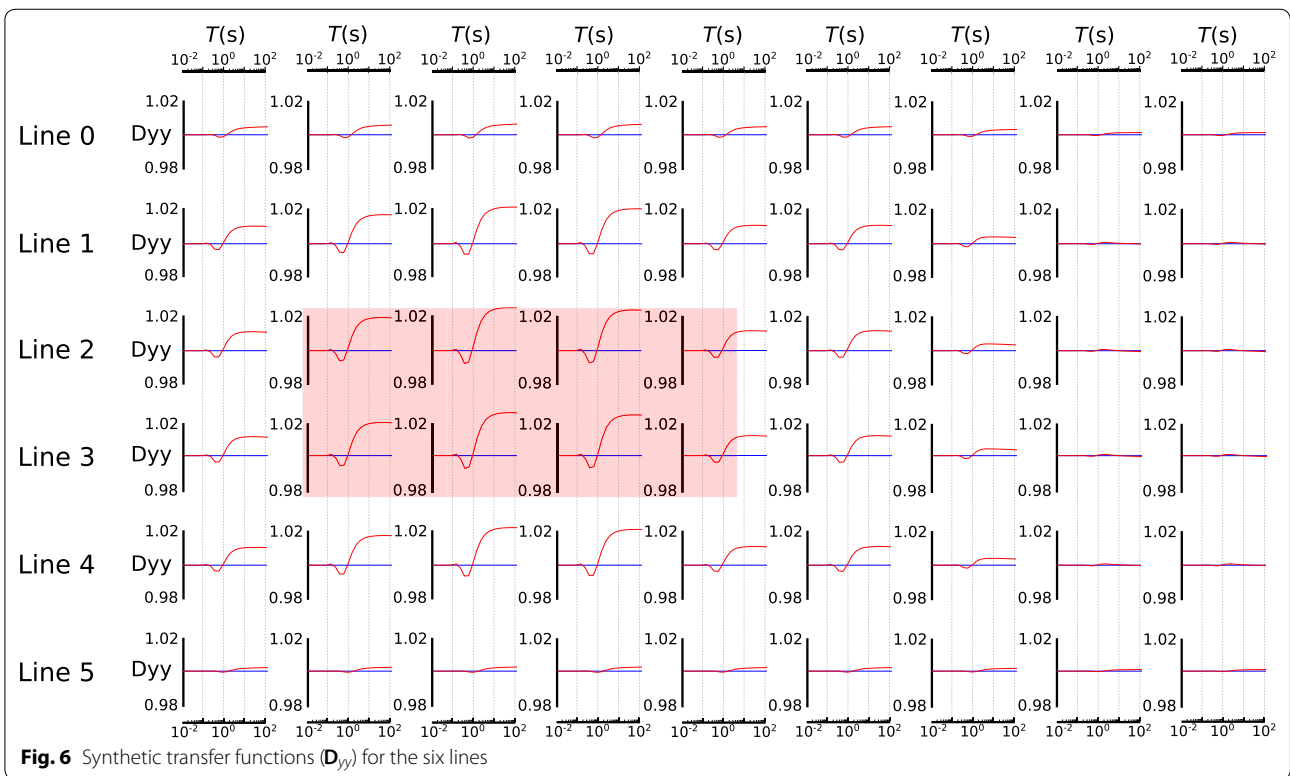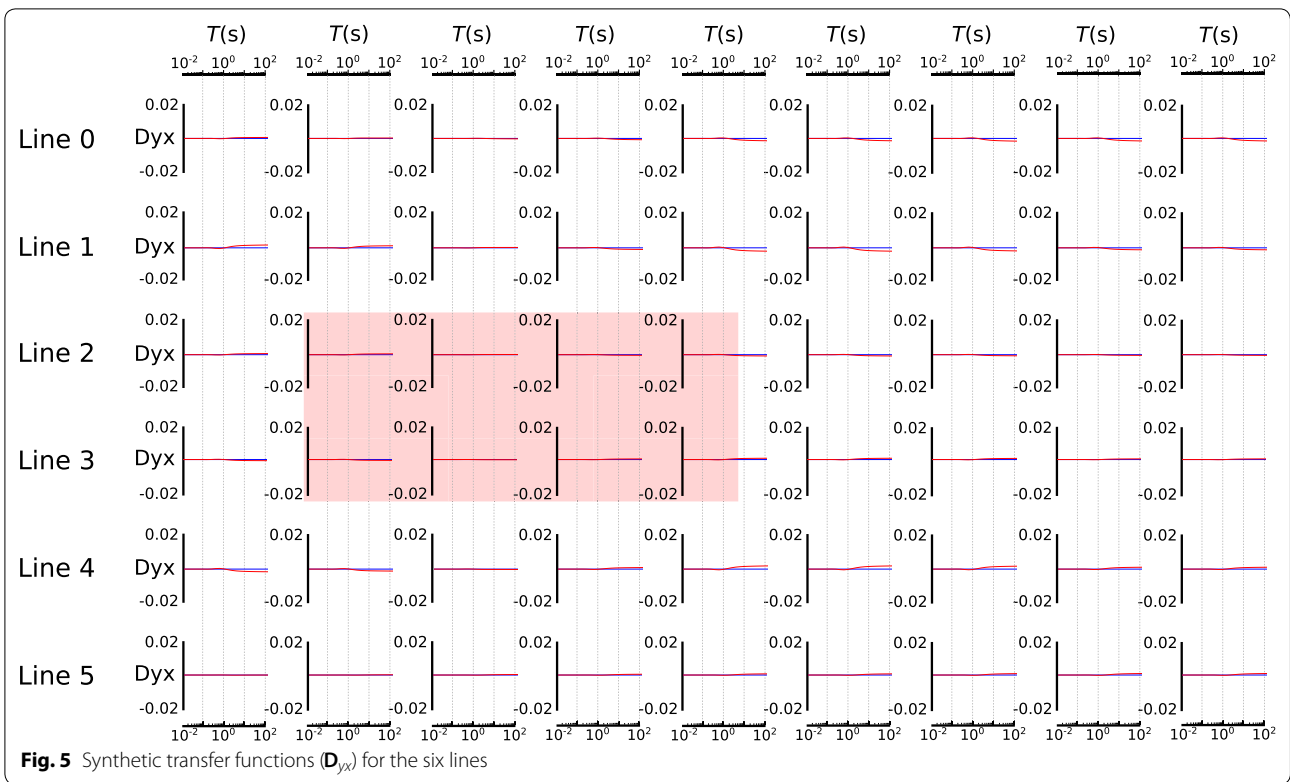
This synthetic study demonstrates different techniques for mapping changes in transfer functions resulting from changes in electric fields caused by hydraulic stimulation. The changes in transfer functions were observed to be in the order of 1–2%, and occurred in D_{xx} and D_{yy}. The changes in D_{xy} and D_{yx} were generally less than 1%. The resultant telluric distortion matrix changes can be analysed using SVD and EA and mapped onto Mohr circle grids. The Mohr circles were found to increase in diameter at periods and areas associated with the conductive anomaly. In order to sufficiently monitor hydraulic stimulation, surveys should be designed such that lines of instruments extend sufficiently beyond the stimulation

zone in both horizontal and (especially) vertical directions. Interpretations regarding the extent of the stimulation should be conservative and take into account the lack of cross-line constraint. In general, changes in telluric distortion resulting from hydraulic fracturing are small and for a real survey it may be difficult to see such changes due to noise in $\mathbf{E}_B$ and $\mathbf{E}_M$.

Example from Paralana, South Australia
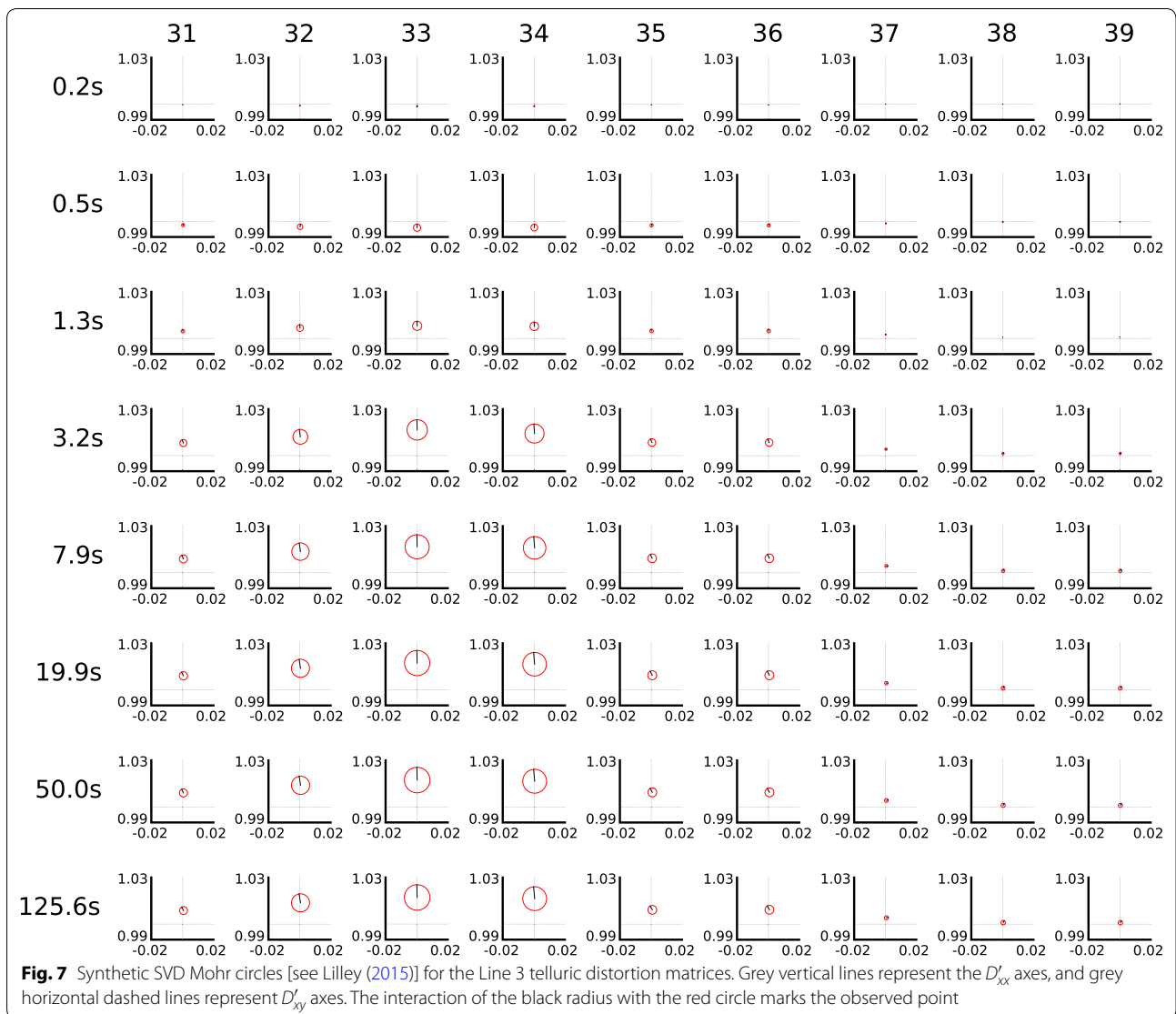
In July 2011, Peacock et al. (2013) conducted a magnetotelluric (MT) survey in Paralana, South Australia, with the aim of continuously monitoring changes in MT responses associated with the introduction of saline hydraulic fracturing fluids at depth. The test site was a geothermal reservoir containing hot granites, with the heat source coming from radiogenic elements within the

Rees *et al. Earth, Planets and Space* (2018) 70:7

Page 5 of 12

Fig. 3 Synthetic transfer functions (**D**$_{xx}$) comparing base (orange dashed box in Fig. 2) and measured (purple dashed box in Fig. 2) sites for Lines 1–6. The *x*-axis is the period in seconds. The blue transfer functions represent the baseline model, and red transfer functions result from the introduction of the 1 Ωm conductive body at 3.6 km depth (represented by the red shaded rectangle). Note that only the real components of the transfer functions are plotted

Fig. 4 Synthetic transfer functions (**D**$_{xy}$) for the six lines

Rees *et al. Earth, Planets and Space* (2018) 70:7

Page 6 of 12

Fig. 5 Synthetic transfer functions ($\mathbf{D}_{yx}$) for the six lines

Fig. 6 Synthetic transfer functions ($\mathbf{D}_{yy}$) for the six lines

Rees *et al. Earth, Planets and Space* (2018) 70:7

Page 7 of 12

Fig. 7 Synthetic SVD Mohr circles [see Lilley (2015)] for the Line 3 telluric distortion matrices. Grey vertical lines represent the D'_{xx} axes, and grey horizontal dashed lines represent D'_{xy} axes. The interaction of the black radius with the red circle marks the observed point
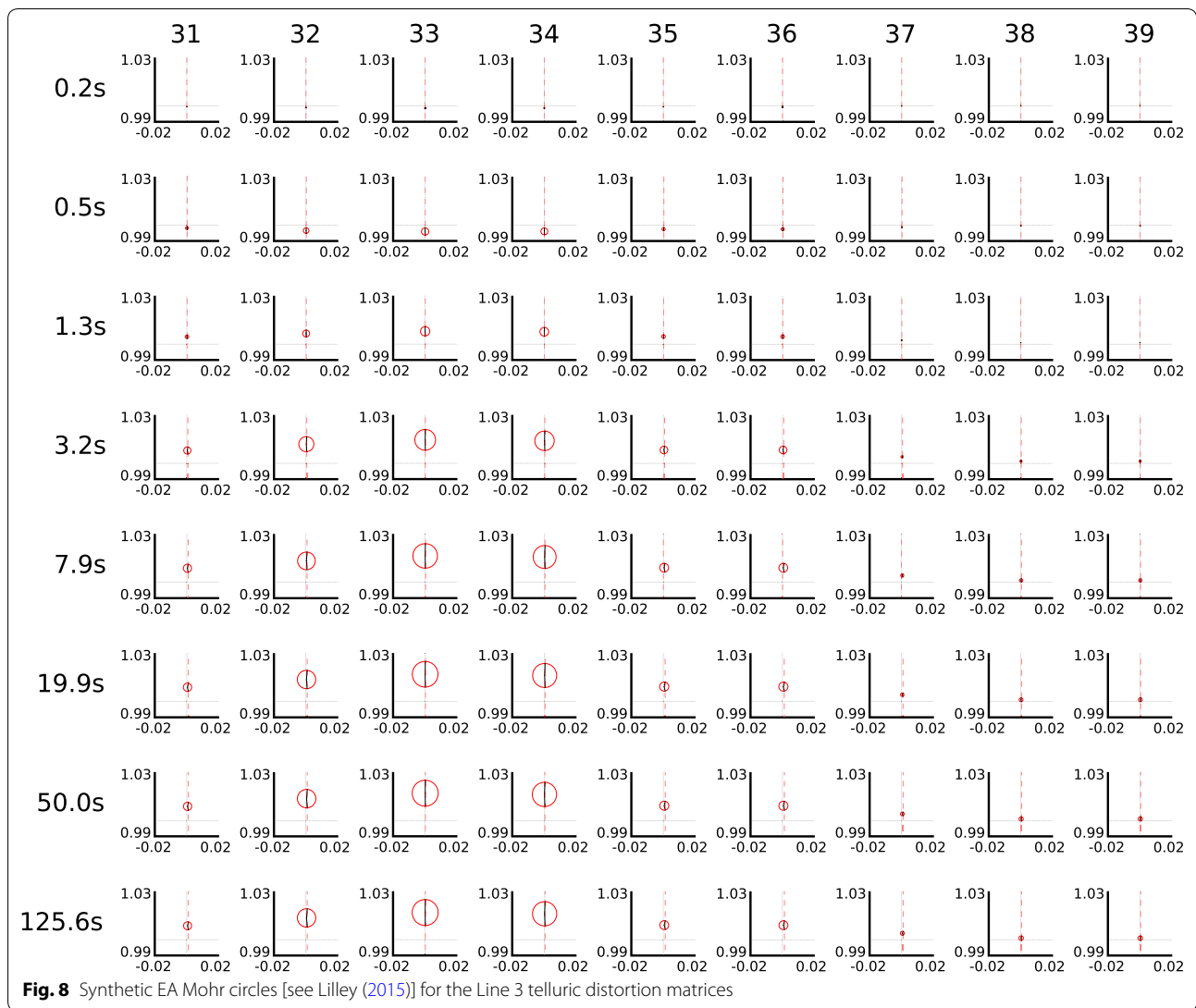
Paleoproterozoic to Mesoproterozoic gneiss, granites and metasediments of the Mount Painter Domain that underlay the Flinders Rangers (McLaren et al. 2003; Brugger et al. 2005). 3.1 million litres of saline water (resistivity of 0.3 Ωm) was injected at a depth of 3680 m, with the injection beginning on day 193 at 0400 universal time (UT) and taking 4 days to complete (Peacock et al. 2012). The survey layout is shown in Fig. 10, with the microseismic cloud visible in the bottom right corner.

Phase tensor (PT) and resistivity tensor (RT) residuals were used as a diagnostic tool for determining directional fluid migration. The changes observed in residual PT and RT were interpreted as fracturing fluids migrating towards the northeast of the injection well along an existing fault system trending north-northeast. This section attempts to analyse the impedance matrix **D** (calculated from the electric fields) from the Paralana experiment to determine whether electric fields alone can be used to monitor hydraulic stimulation at depth.

For this study, station 04 is used as the measured electric field ($\mathbf{E}_M$) and stations 13 and 27 as the base electric fields ($\mathbf{E}_B$). Each station recorded responses during the hydraulic stimulation from days 193–197 (see Additional File 1. Note that day 195 was excluded as the signal strength was low and hence the responses are dominated by noise). Transfer functions comparing stations 13 ($\mathbf{E}_B$) and 04 ($\mathbf{E}_M$) over the stimulation time interval are shown in Fig. 11. The grey shaded area represents the MT dead band, where signal power is naturally low, especially from 2009 to 2011 (Peacock et al. 2013). The blue horizontal lines represent the theoretical baseline transfer functions, with the pink shaded area representing a 1% noise uncertainty.

Rees *et al. Earth, Planets and Space* (2018) 70:7

Page 8 of 12

Fig. 8 Synthetic EA Mohr circles [see Lilley (2015)] for the Line 3 telluric distortion matrices
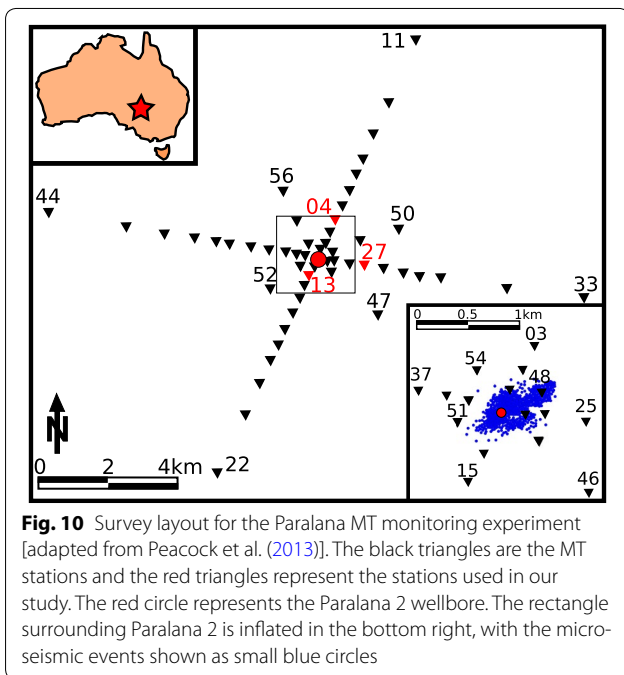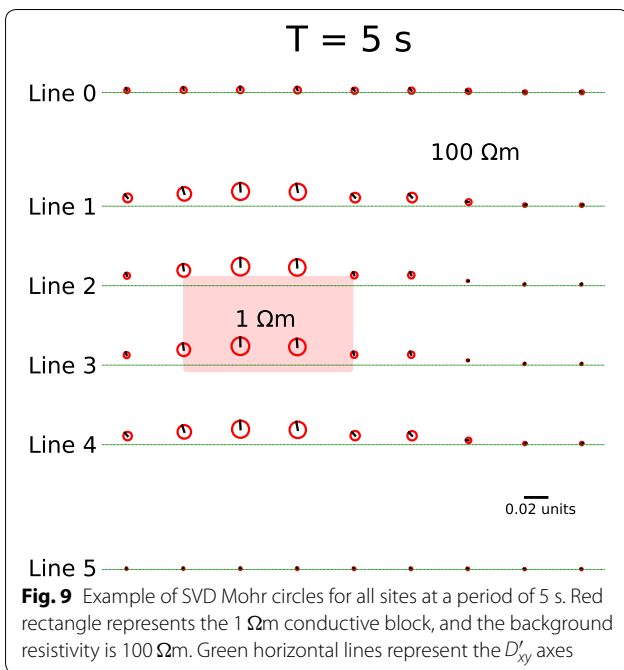
Note that only the real components of the transfer functions are plotted. D_{yy} shows similar behaviour to the feasibility study, where increases of approximately 2% above the noise window occur from 5 s and continue to longer periods for all days. D_{yx} is mostly within the $\pm 1\%$ noise window for all days. D_{xy} shows an almost 5% increase on day 194, with the other days mostly within the noise window. Finally, D_{xx} decreases by $< 1\%$ on days 193 and 196.

Transfer functions comparing stations 27 ($\mathbf{E}_B$) and 04 ($\mathbf{E}_M$) over the same time interval are shown in Fig. 12. Similar trends to Fig. 11 are observed, where an increase in D_{yy} exists in the order of 5% from 5 s to longer periods for all days. D_{xy} shows a 2% increase over a similar period range to D_{yy}. Both D_{xx} and D_{xy} are within the noise windows for most days.
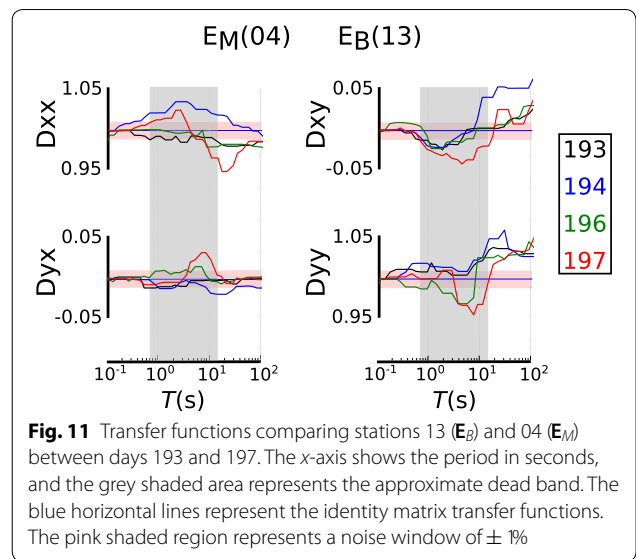
SVD and EA is performed on the telluric distortion matrices for the four days, with the results plotted onto Mohr circle grids as shown in Figs. 13 and 14, respectively. Although the site noise and dead band add complexities to the analysis, the general trend shows the Mohr circles increase in diameter for periods greater than 5 s. When comparing stations 04 and 27, an interesting trend exists for periods between 2 and 14 s, where the Mohr circles progressively increase in diameter over the length of the pumping interval. EA shows eigenvalues that are real and different, with eigenvectors trending orthogonally indicating the telluric distortion matrix is close to 2D. This differs when comparing stations 04 and 13 where the eigenvectors are real but not orthogonal, which may be indicative of a general 3D structure.
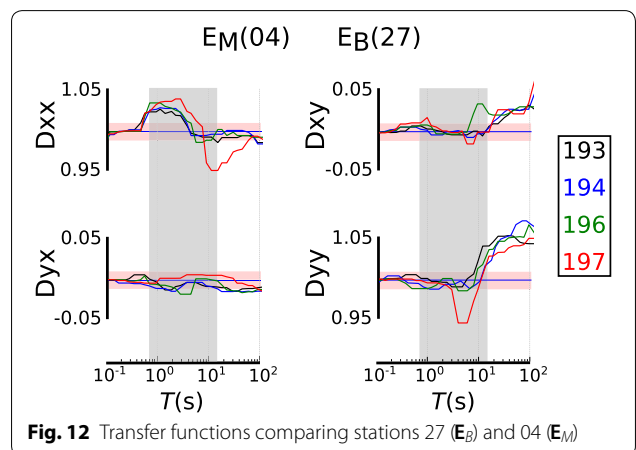
Rees *et al. Earth, Planets and Space* (2018) 70:7

Page 9 of 12

Fig. 9 Example of SVD Mohr circles for all sites at a period of 5 s. Red rectangle represents the 1 Ωm conductive block, and the background resistivity is 100 Ωm. Green horizontal lines represent the D'_{xy} axes

Fig. 10 Survey layout for the Paralana MT monitoring experiment [adapted from Peacock et al. (2013)]. The black triangles are the MT stations and the red triangles represent the stations used in our study. The red circle represents the Paralana 2 wellbore. The rectangle surrounding Paralana 2 is inflated in the bottom right, with the microseismic events shown as small blue circles
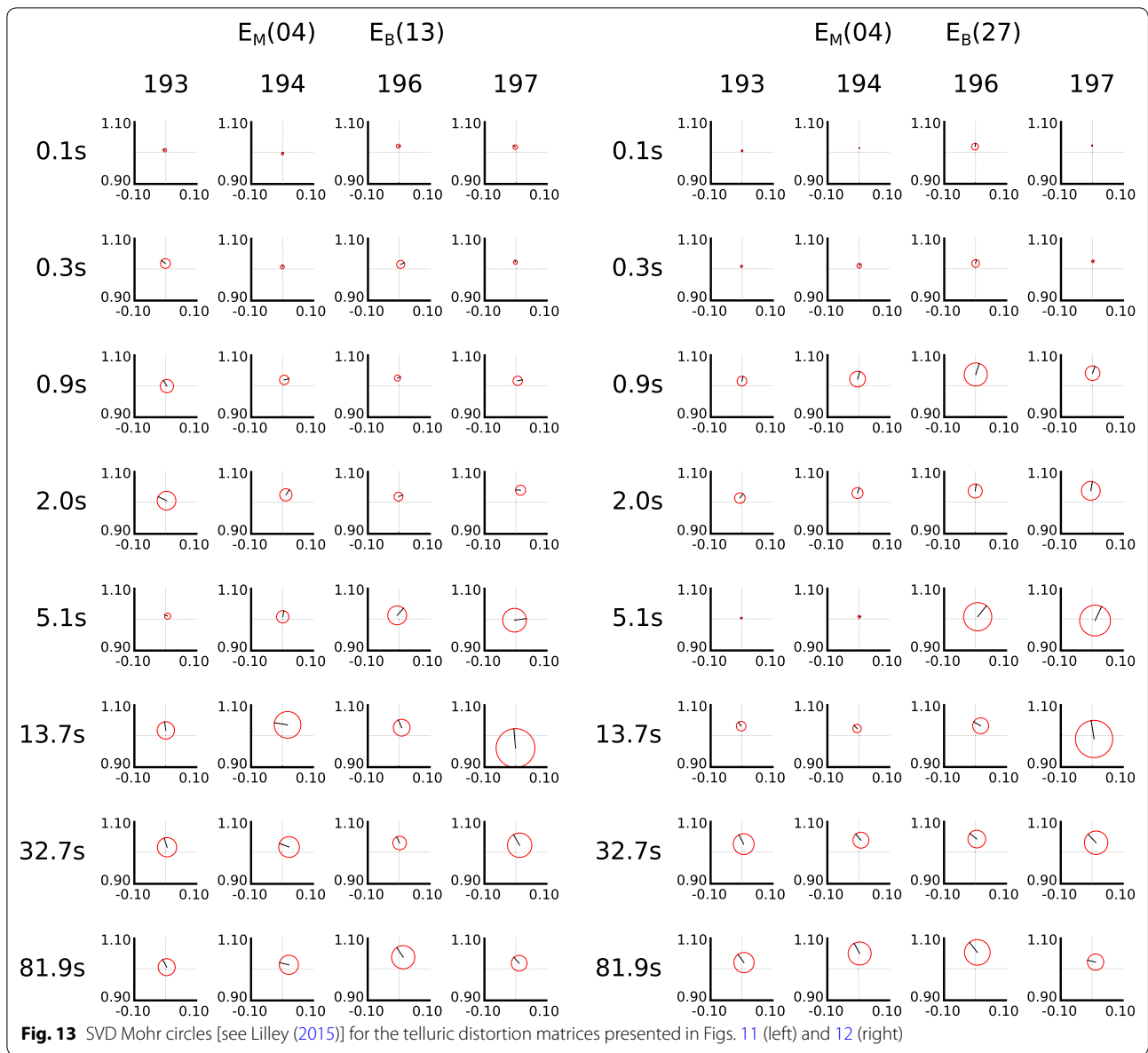
Discussion and conclusion

We have designed and conducted a feasibility study to determine the potential for using the TS method to monitor changes in resistivity structure of the Earth resulting from hydraulic stimulation. Three-dimensional forward modelling of our base and stimulation resistivity structures showed changes in **D** of between 1 and 2% as a

Fig. 11 Transfer functions comparing stations 13 (**E**$_B$) and 04 (**E**$_M$) between days 193 and 197. The x-axis shows the period in seconds, and the grey shaded area represents the approximate dead band. The blue horizontal lines represent the identity matrix transfer functions. The pink shaded region represents a noise window of ± 1%

result of introducing a $3 \times 1 \times 0.4$ km conductive body at 3.6 km depth. The transfer functions were mapped onto a grid by comparing each measured station to a reference (or base) station. Eigenanalysis and singular value decomposition were performed on the telluric distortion matrices from each station at various periods, and plotted onto Mohr circle grids. The resultant grids showed circles increasing in diameter at sites and periods associated with the conductive body. Moving away from the conductive body, the circles progressively approach the identity matrix indicating no telluric distortion had occurred.

The Paralana electric field data were relatively noisy and affected by the dead band making interpretations difficult. D_{xx} and D_{yx} components showed little change from the theoretical transfer functions. D_{xy} and D_{yy} were increasing by 2–5% for periods greater than 5 s. Changes in the
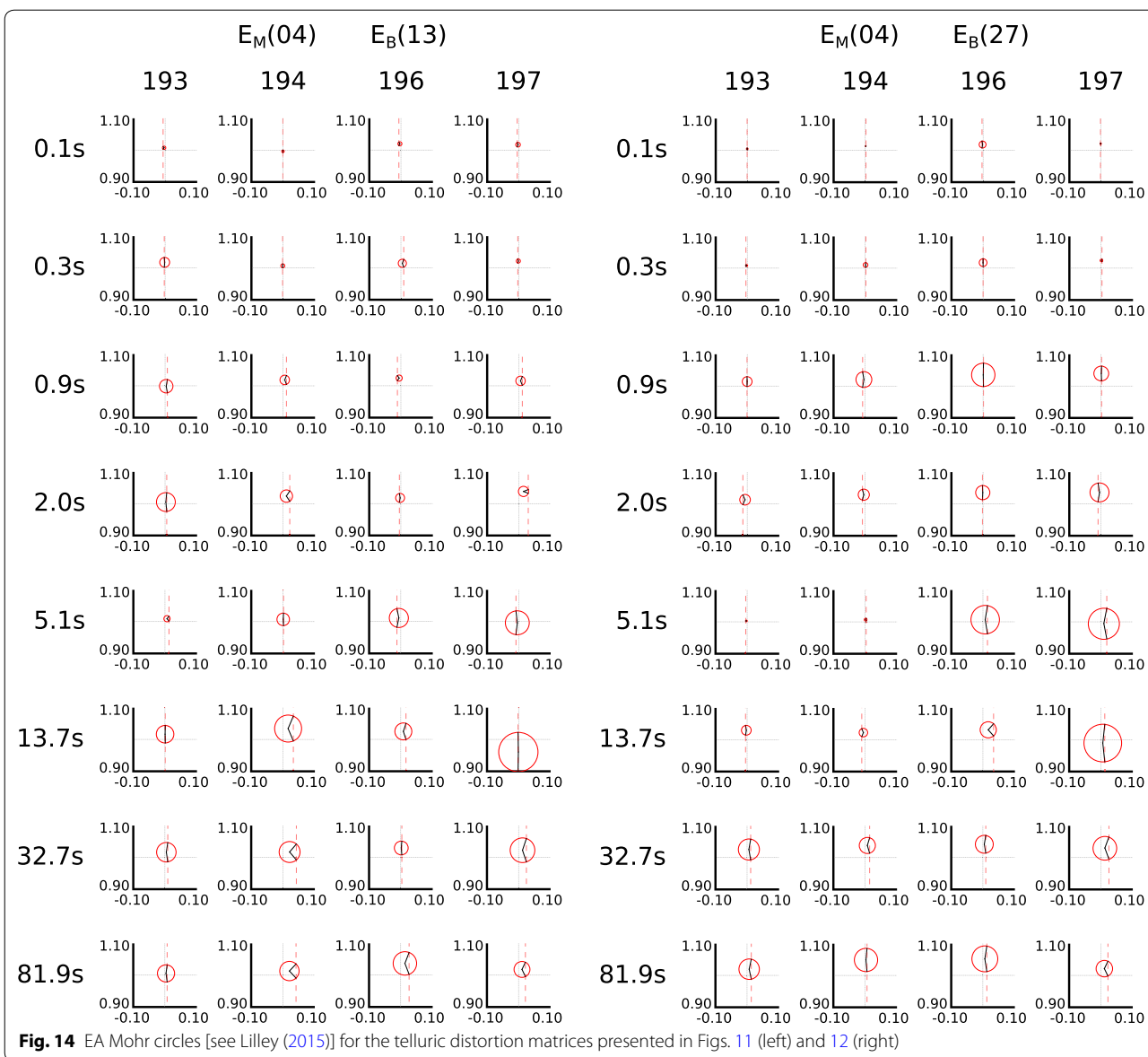

Fig. 12 Transfer functions comparing stations 27 (**E**$_B$) and 04 (**E**$_M$)

Rees *et al. Earth, Planets and Space* (2018) 70:7

Page 10 of 12

Fig. 13 SVD Mohr circles [see Lilley (2015)] for the telluric distortion matrices presented in Figs. 11 (left) and 12 (right)

y-direction are significant but in the *x*-direction are not, suggesting the response is more complex and possibly anisotropic (MacFarlane et al. 2014). Mohr circle grids visualised these changes in transfer function, with the circle diameters increasing at periods greater than 5 s.

This study has shown some potential for utilising the TS method for monitoring subsurface fluid movement. The advantage of this technique is that electric fields are relatively cheap and easy to measure when compared with traditional magnetotelluric surveys. Additionally, this technique can be used for near real-time monitoring from a remote location. However, electric fields are more complex and noisier than magnetics making interpretation more challenging. The

impedance matrix transfer functions are largely real rather than being complex numbers and, in principal for a 1D Earth, are the identity matrix at all periods ($\pm$ static shift). Therefore changes in the earth resulting from the introduction of conductive bodies can be associated with deviations away from the identity matrix. SVD and EA can reduce the complexity of the telluric distortion matrix to simpler parameters that can be visualised in the form of Mohr circles. Grids of Mohr circles may be a useful diagnostic tool for understanding the extent of fluid movement resulting from hydraulic stimulation at depth. However, deep monitoring is always going to be marginal and for depths in the order of 4 km, changes in transfer functions are

Rees *et al. Earth, Planets and Space* (2018) 70:7

Page 11 of 12

Fig. 14 EA Mohr circles [see Lilley (2015)] for the telluric distortion matrices presented in Figs. 11 (left) and 12 (right)

small. Therefore, in order to have meaningful interpretations, electric field data need to be of a high quality with low levels of site noise. Additionally, the dead band affects the transfer functions significantly so a controlled source may be useful for monitoring at depths incorporating dead band periods. Real data examples from depths shallower than the dead band may prove more suitable for determining distinguishable changes in the telluric distortion matrix resulting from the introduction of conductive fluids.

Additional files

Additional file 1. EDI files for both the 3D feasibility study and Paralana example.

Author details
[1] The Australian National University, Canberra, ACT 0200, Australia. [2] The University of Adelaide, Adelaide, SA 5005, Australia.

Competing interests
The authors declare that they have no competing interests.

Availability of data and materials
Included in Additional file.

Rees *et al. Earth, Planets and Space* (2018) 70:7

Page 12 of 12

References
Berdičevskij MN, Keller GV (1965) Electrical prospecting with the telluric current method. Colorado School of Mines, Colorado
Brugger J, Long N, McPhail D, Plimer I (2005) An active amagmatic hydrothermal system: the Paralana hot springs, northern flinders ranges, South Australia. Chem Geol 222:35–64
Chave AD, Jones AG (2012) The magnetotelluric method: theory and practice. Cambridge University Press, Cambridge
Chave AD, Smith JT (1994) On electric and magnetic galvanic distortion tensor decompositions. J Geophys Res Solid Earth 99:4669–4682
Groom RW, Bailey RC (1989) Decomposition of magnetotelluric impedance tensors in the presence of local three-dimensional galvanic distortion. J Geophys Res Solid Earth 94:1913–1925
Lilley F (1993) Magnetotelluric analysis using Mohr circles. Geophysics 58:1498–1506
Lilley F (2012) Magnetotelluric tensor decomposition: insights from linear algebra and Mohr diagrams. In: Lim HS (ed) New achievements in geoscience. InTech Open Science, Rijeka, pp 81–106
Lilley F (2015) The distortion tensor of magnetotellurics: a tutorial on some properties. Explor Geophys 47:85–99
MacFarlane J, Thiel S, Pek J, Peacock J, Heinson G (2014) Characterisation of induced fracture networks within an enhanced geothermal system using anisotropic electromagnetic modelling. J Volcanol Geotherm Res 288:1–7
Mackie RL, Madden TR, Wannamaker PE (1993) Three-dimensional magnetotelluric modeling using difference equations-theory and comparisons to integral equation solutions. Geophysics 58:215–226
McLaren S, Sandiford M, Hand M, Neumann N, Wyborn L, Bastrakova I (2003) The hot southern continent: heat flow and heat production in Australian Proterozoic terranes. Geol Soc Am Spec Papers 372:157–167
Peacock J, Thiel S, Reid P, Heinson G (2012) Magnetotelluric monitoring of a fluid injection: example from an enhanced geothermal system. Geophys Res Lett 39:L18403. https://doi.org/10.1029/2012GL053080
Peacock JR, Thiel S, Heinson GS, Reid P (2013) Time-lapse magnetotelluric monitoring of an enhanced geothermal system. Geophysics 78:B121–B130
Yungul S (1966) Telluric sounding—a magnetotelluric method without magnetic measurements. Geophysics 31:185–191